IJMMM International Journal of Minerals, Metallurgy and Materials 矿物冶金与材料学报（英文版）

Depression mechanism of sulfite ions on sphalerite and Pb^{2+} activated sphalerite in the flotation separation of galena from sphalerite

Feng Zhang, Chenyang Zhang, Linlin Wu, Wei Sun, Hongliang Zhang, Jianhua Chen, Yong Pei, and Songjiang Li

Cite this article as:
Feng Zhang, Chenyang Zhang, Linlin Wu, Wei Sun, Hongliang Zhang, Jianhua Chen, Yong Pei, and Songjiang Li, Depression mechanism of sulfite ions on sphalerite and Pb^{2+} activated sphalerite in the flotation separation of galena from sphalerite, *Int. J. Miner. Metall. Mater.*, 32(2025), No. 2, pp. 335-345. https://doi.org/10.1007/s12613-024-2936-2

Articles you may be interested in

Tichen Wang, Guiju Sun, Jiushuai Deng, Hongxiang Xu, Guoyong Wang, Mingzhen Hu, Qizheng Qin, and Xiaohao Sun, A depressant for marmatite flotation: Synthesis, characterisation and floatation performance, *Int. J. Miner. Metall. Mater.*, 30(2023), No. 6, pp. 1048-1056. https://doi.org/10.1007/s12613-022-2586-1

Qiancheng Zhang, Limin Zhang, Feng Jiang, Honghu Tang, Li Wang, and Wei Sun, Ferric ion-triggered surface oxidation of galena for efficient chalcopyrite–galena separation, *Int. J. Miner. Metall. Mater.*, 31(2024), No. 2, pp. 261-267. https://doi.org/10.1007/s12613-023-2674-x

Haiyun Xie, Jialing Chen, Pei Zhang, Likun Gao, Dianwen Liu, and Luzheng Chen, Separation of galena and chalcopyrite using the difference in their surface acid corrosion characteristics, *Int. J. Miner. Metall. Mater.*, 30(2023), No. 11, pp. 2157-2168. https://doi.org/10.1007/s12613-023-2654-1

Lei Tian, Ao Gong, Xuan-gao Wu, Yan Liu, Zhi-feng Xu, and Ting-an Zhang, Cu^{2+}-catalyzed mechanism in oxygen-pressure acid leaching of artificial sphalerite, *Int. J. Miner. Metall. Mater.*, 27(2020), No. 7, pp. 910-923. https://doi.org/10.1007/s12613-019-1918-2

Chao Gu, Ziyu Lyu, Qin Hu, and Yanping Bao, Investigation of the structural, electronic and mechanical properties of CaO–SiO_2 compound particles in steel based on density functional theory, *Int. J. Miner. Metall. Mater.*, 30(2023), No. 4, pp. 744-755. https://doi.org/10.1007/s12613-022-2588-z

Qicheng Feng, Wenhang Yang, Maohan Chang, Shuming Wen, Dianwen Liu, and Guang Han, Advances in depressants for flotation separation of Cu–Fe sulfide minerals at low alkalinity: A critical review, *Int. J. Miner. Metall. Mater.*, 31(2024), No. 1, pp. 1-17. https://doi.org/10.1007/s12613-023-2709-3

IJMMM WeChat

QQ author group

INTERNATIONAL JOURNAL OF
Minerals, Metallurgy and Materials

Volume 32, Number 2, February 2025
Page 335

Research Article https://doi.org/10.1007/s12613-024-2936-2

Depression mechanism of sulfite ions on sphalerite and Pb^{2+} activated sphalerite in the flotation separation of galena from sphalerite

Feng Zhang[1)], *Chenyang Zhang*[1,2),✉], *Linlin Wu*[3),✉], *Wei Sun*[1)], *Hongliang Zhang*[1)], *Jianhua Chen*[4)], *Yong Pei*[2,5)], *and Songjiang Li*[6),✉]

1) Engineering Research Center of Ministry of Education for Carbon Emission Reduction in Metal Resource Exploitation and Utilization, Hunan International Joint Research Center for Efficient and Clean Utilization of Critical Metal Mineral Resources, School of Minerals Processing and Bioengineering, Central South University, Changsha 410083, China

2) State Key Laboratory of Mineral Processing, Beijing General Research Institute of Mining & Metallurgy, Beijing 100160, China

3) Hunan Provincial Key Laboratory of Micro & Nano Materials Interfaces Science, College of Chemistry and Chemical Engineering, Central South University, Changsha 410083, China

4) School of Resources, Environment and Materials, Guangxi University, Nanning 530004, China

5) Department of Chemistry, Xiangtan University, Xiangtan 411105, China

6) China Railway Resource Group Co. Ltd, Beijing 102300, China

(Received: 22 February 2024; revised: 14 May 2024; accepted: 17 May 2024)

Abstract: The depression mechanism of sulfite ions on sphalerite and Pb^{2+} activated sphalerite in the flotation separation of galena from sphalerite still lacked in-depth insight. Therefore, the depression mechanism of sulfite ions on sphalerite and Pb^{2+} activated sphalerite in the flotation separation of galena from sphalerite was further systematically investigated with experiments and density functional theory (DFT) calculations. The X-ray photoelectric spectroscopy (XPS) results, DFT calculation results, and frontier molecular orbital analysis indicated that sulfite ions were difficult to be adsorbed on sphalerite surface, suggesting that sulfite ions achieved depression effects on sphalerite through other non-adsorption mechanisms. First, the oxygen content in the surface of sphalerite treated with sulfite ions increased, which enhanced the hydrophilicity of the sphalerite and further increased the difference in hydrophilicity between sphalerite and galena. Then, sulfite ions were chelated with lead ions to form $PbSO_3$ in solution. The hydrophilic $PbSO_3$ was more easily adsorbed on sphalerite than galena. The interaction between sulfite ions and lead ions could effectively inhibit the activation of sphalerite. In addition, the UV spectrum showed that after adding sulfite ions, the peak of perxanthate in the sphalerite treated xanthate solution was significantly stronger than that in the galena with xanthate solution, indicating that xanthate interacted more readily with sulfite ions and oxygen molecules within the sphalerite system, leading to the formation of perxanthate. However, sulfite ions hardly depressed the flotation of galena and could promote the flotation of galena to some extent. This study deepened the understanding of the depression mechanism of sulfite ions on sphalerite and Pb^{2+} activated sphalerite.

Keywords: sphalerite; galena; sulfite ion; density functional theory; depression mechanism

1. Introduction

Inorganic depressants are important in inhibiting sphalerite flotation due to their lower cost than organic depressants. Commonly used inorganic depressants include cyanide, lime, zinc sulfate, sodium sulfide, sulfite, and their respective salts [1]. Cyanide exhibits strong inhibitory effect on sphalerite but does not affect galena. However, its environmental toxicity limits its application in Pb–Zn flotation [2–3]. Lime and zinc sulfate inhibit sphalerite by forming a hydrophilic film on its surface [1,4–6]. Sodium sulfide also demonstrates inhibitory properties against sphalerite [7–8]. Sulfite and its salts are typically utilized in combination with zinc sulfate and other depressants, offering several advantages such as low toxicity, insoluble gold and silver, and enhanced activation of Cu^{2+} [1,9–11].

Extensive research conducted by scholars has shed light on the inhibitory mechanism of sulfite and its salts on minerals, contributing significantly to the development of the basic theory of mineral flotation. For instance, Khmeleva *et al*. [12] investigated the flotation mechanism of sodium bisulfite in the absence of collectors for inhibiting copper activation of sphalerite. They found that sulfate ions interacted with copper-activated pyrite, leading to the breakdown of hydrophobic sulfur compounds essential for the flotation process. Furthermore, Khmeleva *et al*. [11] explored the inhibitory

✉ Corresponding authors: Chenyang Zhang E-mail: zhangchenyang@csu.edu.cn; Linlin Wu E-mail: chemwll@csu.edu.cn; Songjiang Li E-mail: minengine@163.com

Springer

mechanism of sodium bisulfite on copper-activated sphalerite in the presence of xanthate. They proposed that the decomposition of copper xanthate and hydrophobic copper sulfide compounds caused by sulfurous acid was the main mechanism for its inhibition of sphalerite.

In addition, the use of sodium sulfite to enhance the separation of copper-activated sphalerite and pyrite under weakly alkaline pH conditions was demonstrated by Shen *et al*. [13]. Spectral research results indicated that sodium sulfite promoted the oxidation of copper on pyrite, forming copper hydroxide, but had no effect on sphalerite. Khmeleva *et al*. [14] also investigated the depression mechanism of sulfite on copper-activated pyrite in the presence of xanthate. They determined that the depression effect of sulfite on copper-activated pyrite, in the presence of xanthate, entailed four mechanisms: (1) xanthate decomposition through perxanthate formation in solution; (2) desorption of di-xanthogen from the pyrite surface; (3) consumption of dissolved oxygen by sulfite ions leading to a drop in pulp redox potential; (4) pyrite oxidation by sulfite ions renders its mineral surface hydrophilic. Additionally, Grano *et al*. [15] examined the effect of sulfite on galena flotation. The formation of insoluble lead sulfite precipitates on the galena's surface was affirmed by the dissolution study of the galena and X-ray photoelectron spectroscopy (XPS) examination of its surface. However, sulfite did not completely inhibit xanthate adsorption at these specific sites, thus explaining the relatively weak inhibition of sulfite on galena flotation. The depression mechanism of sulfite and its salts was generally considered intricate.

Previous studies predominantly focused on the depression mechanism of sulfite ions on copper ions activated sphalerite, suggesting that sulfite ions decompose hydrophobic sulfur compounds and copper xanthate, thereby depressing copper ions activated sphalerite. However, the depression mechanism of sulfite ions on sphalerite and Pb^{2+} activated sphalerite to separate galena from sphalerite remained unclear. It was essential to determine whether the depression of sphalerite by sulfite ions was solely due to their adsorption or if other ways were involved. This work aimed to further investigate the depression mechanism of sulfite ions on sphalerite and Pb^{2+} activated sphalerite in the separation of galena from sphalerite, employing various characteriazations to gain comprehensive understanding of sulfite's intricate role in Pb–Zn flotation.

2. Experimental

2.1. Materials

2.1.1. Mineral samples and reagents

Pure galena and sphalerite samples were obtained from Hunan province, China. The samples were initially ground and screened, and the particle size of 38–74 μm fraction was selected for micro-flotation, ultraviolet–visible (UV–vis) spectrum, and Fourier transform infrared (FTIR) spectroscopy. Furthermore, the particle sizes below 38 μm were subjected to additional grinding for 30 min to prepare the XPS samples. Fig. 1 demonstrated the high purity of the mineral samples, confirming their suitability for the respective experimental analyses. The chemicals employed in the experiment, including hydrochloric acid, sodium hydroxide, sodium sulfite, and sodium butyl xanthate (SBX), were all of analytical purity.

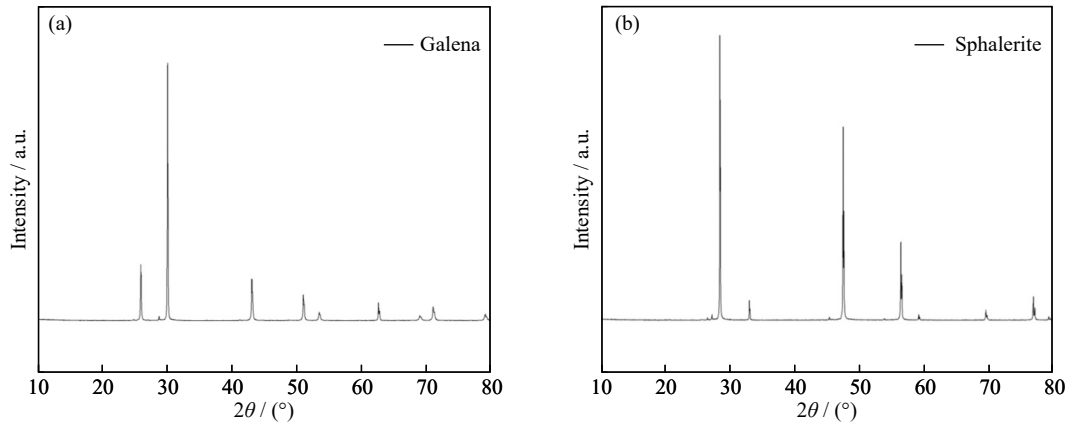

Fig. 1. X-ray diffraction (XRD) patterns of (a) galena and (b) sphalerite samples.

2.1.2. Solution chemical analysis

The solution composition of sulfite ions was calculated by Visual MINTEQ software [16]. The calculation parameters were set as the concentration of SO_3^{2-} 30 mg/L at 25°C. The pH was changed from 0 to 14. From Fig. 2, it could be observed that when the pH value was between 3 and 6, the component of the sulfite solution was mainly HSO_3^-. When the pH was larger than 8, the main component in the sulfite solution was SO_3^{2-}. By analyzing the concentration components in the sulfite solution, the configuration of sulfite ions was determined to simulate the adsorption of sulfite ions on mineral surfaces in alkaline environments.

2.2. Methodology

2.2.1. Micro-flotation tests

Investigations on mineral flotation were conducted in XFG flotation machine from China. The pure mineral samples (2 g) were cleaned with ultrasonic cleaning device for 3 min to eliminate oxidation film. After that, 40 mL of deionized water was added to the flotation cell together with the

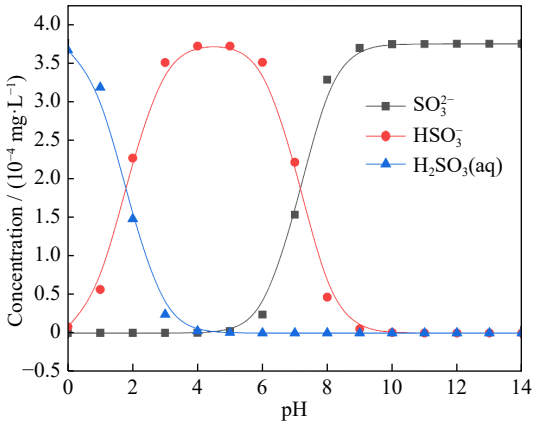

Fig. 2. Effect of pH on species of SO_3^{2-} solution.

ultrasonic-treated samples. The various dosing sequences were as follows: (1) minerals + pH + SBX; (2) minerals + pH + Na_2SO_3 + SBX; (3) minerals + $Pb(NO_3)_2$ + pH + SBX; (4) minerals + $Pb(NO_3)_2$ + pH + Na_2SO_3 + SBX. The pulp's pH was stabilized in 2 min using hydrochloric acid and sodium hydroxide. And all reagents reacted for 2 min. Then, 0.2 μL terpineol was added to the flotation cell for foaming with 1 min, and foam products were collected with scraper for 4 min. Eventually, filter, dry, and weigh foam products and tank bottom products, and calculate the proportion of foam products in the total product quality, that is, the recovery.

When conducting micro-flotation research on binary mixed minerals, 1 g of galena and 1 g of sphalerite were placed into a flotation cell. The dosing sequence of mixed minerals was consistent with that of single minerals. Pb grade in concentrates was detected by chemical element analysis.

2.2.2. Contact angle measurement

A sessile drop approach was used to assess the wettability of mineral surfaces using JY82C contact angle device. In order to obtain fresh surfaces, the well-selected mineral sample was polished using polishing paper. The prepared mineral sample was then immersed in the required solution for 5 min. The corresponding dosing sequences were as follows: (1) minerals + pH (9) + SBX and (2) minerals + Na_2SO_3 + pH (9) + SBX. The contact angle measurement was performed after the treated mineral sample had been dried in the air.

2.2.3. Analysis method

UV-vis spectroscopy was used to determine the adsorption strength of SBX on minerals. Initially, 1 g of 38–74 μm samples and 40 mL distilled water were combined. The various dosing sequences were as follows: (1) minerals + pH (9) + SBX and (2) minerals + Na_2SO_3 + pH (9) + SBX. The concentrations of sodium butyl xanthate and sodium sulfite were 60 and 30 mg/L, respectively. After adding the reagents, the solution was stirred for 10 min. Then, filter the suspension using syringe filter with pore size of 0.45 μm. Finally, the peak intensity of SBX in filtrate was determined using UV-2600 spectrometer. According to the variation in peak intensity, the adsorption strength of SBX on minerals was determined. In addition, in the experiment of sulfite decomposition of Pb-xanthate and Zn-xanthate, 60 mg/L $Pb(NO_3)_2$ or 60 mg/L $ZnSO_4$ was mixed with 60 mg/L butyl sodium xanthate. Then, 30 mg/L sodium sulfite was added to adjust pH to 6. The decomposition rate of xanthate treated with Pb^{2+} and xanthate treated with Zn^{2+} was determined based on the intensity of producing perxanthate [17]. Besides, the concentration of Pb^{2+} and Zn^{2+} in the experiment of precipitation of metal ions with sulfite ions were detected by inductively coupled plasma-optical emission spectrometer (ICP-OES).

2.2.4. FTIR spectroscopy

The infrared spectrum utilized an instrument model IR Affinity. FTIR spectroscopy of minerals was obtained utilizing the KBr method. First, 40 mL of deionized water and 0.5 g of minerals (galena or sphalerite) were introduced in a flotation cell. The different dosing sequences were as follows: (1) minerals + pH (9) + SBX and (2) minerals + Na_2SO_3 + pH (9) + SBX. The pH was adjusted to 9. The concentrations of SBX and Na_2SO_3 put into the beaker were 6000 mg/L. Moreover, the solution was stirred for 1 h. Afterward, the samples were washed three times with pure deionized water to remove leftover SBX. Finally, samples were dehydrated for measurements.

2.2.5. XPS analysis

XPS analysis was conducted in vacuum analytical laboratory utilizing a Thermo Scientific ESCALAB 250Xi system from the United States with Al-K_α as the sputtering source. In this experiment, 40 mL of deionized water and 0.5 g of mineral (galena or sphalerite) samples were combined and put into a 100 mL beaker. The various dosing sequences were as follows: (1) minerals + pH (9); (2) minerals + Na_2SO_3 + pH (9). The pH was adjusted to 9. The sample was then agitated magnetically for 30 min. Then, the suspension was filtered. Clean solid fraction vacuum dried at 40°C to produce a final sample for XPS measurements.

2.2.6. DFT calculations

The DFT calculations were performed with the CASTEP module in the Materials Studio 2017 package [18]. The PW91 functional approximates the exchange-correlation potential of the Generalized Gradient Approximation [19]. To precisely define the weak interactions of the H-bonding interaction and dispersion, DFT-D correction with the Tkatchenko-Scheffler (TS) approach was utilized in all calculations [20–21]. According to previous research, the sphalerite (110) surface was the most stable surface [22–24]. Therefore, the slab model (110) surface was used, which was finally enlarged into 3 × 2 × 1 supercell model. The galena (100) surface was considered to be the universal stable exposed plane [25–26]. The slab model galena (100) surface was used and enlarged into 3 × 3 × 1 supercell model. Then, the slab model of sphalerite (110) surface and galena (100) surface with three thicknesses and 25 Å vacuum layer was structured. The H_2O, SO_3^{2-}, and $PbSO_3$ were pre-optimized in a cubic cell of 20 Å × 20 Å × 20 Å using the *k*-point of Gamma and cutoff energy of 400 eV. For the surface model, *k*-point meshes of 1 × 1 × 1 and cutoff energy of 370 eV were also employed. The Mg^{2+} were used to balance the charge of SO_3^{2-} in the system. The convergence tolerance of self-consistent field interaction was 1 × 10^{-6} eV/atom. The convergence tolerances of energy,

maximum force, maximum stress, and maximum displacement were set as 2×10^{-5} eV/atom, 0.05 eV/Å, 0.1 GPa, and 2×10^{-3} Å, respectively.

The adsorption performance of various flotation reagents on mineral surfaces can be effectively evaluated by adsorption energy. The adsorption energy (E_{ads}) is calculated using the following formula [27–28]:

$$E_{ads} = E_{system} - E_{slab} - E_{adsorbates},$$

where E_{system} is the energy of the system, and E_{slab} and $E_{adsorbates}$ are denoted as the energies of the slab model and adsorbates, respectively.

3. Results and discussion

3.1. Micro-flotation experiments

3.1.1. Single mineral flotation

Galena and sphalerite were subjected to single mineral flotation tests to assess the floatability with and without Na_2SO_3. Fig. 3 depicted that sphalerite's recovery reached approximately 20% under acidic conditions when SBX collector dosage was 60 mg/L. As pH increased, sphalerite's recovery gradually decreased, and it couldn't be floated at pH = 9. Conversely, galena exhibited consistent floatability across the entire pH range. The addition of Na_2SO_3 further reduced sphalerite's recovery but slightly enhanced galena's floatability. To investigate if sulfite had a promoting effect on galena flotation, Fig. 4 showed the flotation recovery outcomes for two different particle size of galena in relation to sodium sulfite concentration. At the xanthate concentration of 15 mg/L and pH = 9, both particle size of galena experienced increased flotation recovery as sodium sulfite concentration rose. The recovery at higher concentrations. These findings indicated that sodium sulfite promoted galena recovery in the presence of xanthate.

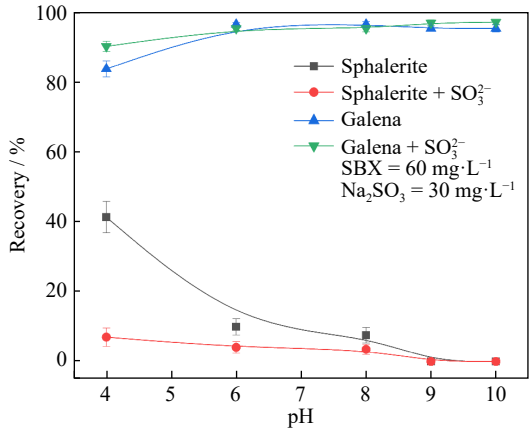

Fig. 3. Flotation recoveries of galena and sphalerite as a function of pH.

During the grinding process, metal ions such as Cu^{2+}, Pb^{2+}, and Ag^{+} are inevitably generated, activating sphalerite [29–32]. This experiment focused on the complexation effect of sulfite ions on Pb^{2+}. Fig. 5 demonstrated that Pb^{2+} strongly activated sphalerite, elevating its recovery by approximately 50% [33]. This was attributed that as pH increased, hydroxide ions in the solution also rose, and Pb^{2+} reacted with hydroxide ions to form hydrophilic lead hydroxide precipitates, reducing sphalerite recovery activated by lead ions. However, the addition of Na_2SO_3 significantly suppressed sphalerite activated with Pb^{2+}. Under acidic conditions, the recovery of Pb^{2+} activated sphalerite decreased by approximately 30%. Under alkaline conditions, the number of free Pb^{2+} decreased. Therefore, the depression effect of sulfite ions on Pb^{2+} activated sphalerite was weakened. Overall, sulfite ions readily formed precipitation products with Pb^{2+}, effectively nullifying the activation effect on sphalerite.

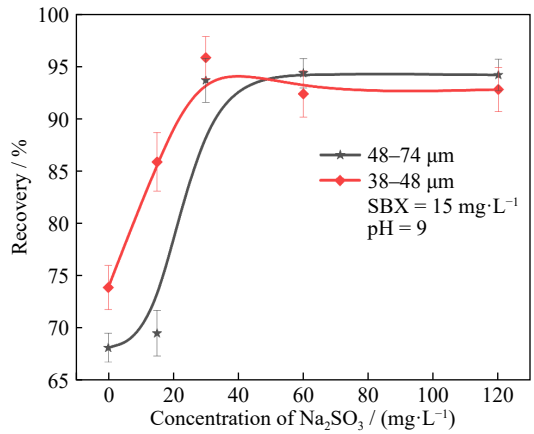

Fig. 4. Flotation recoveries of galena as a function of concentration of Na_2SO_3.

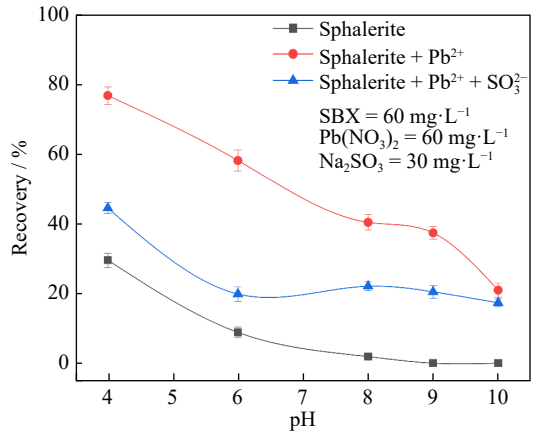

Fig. 5. Flotation recoveries of sphalerite activated by Pb^{2+} as a function of pH.

3.1.2. Flotation experiment of binary mixed minerals

Binary mixed mineral tests were conducted to confirm the role of sulfite ions in Pb–Zn mineral separation under alkaline conditions. Fig. 6(a) showed the separation of Pb–Zn binary mixture with sulfite ions without the addition of Pb^{2+}. Without Na_2SO_3, the concentrate achieved a yield of 49.30% and Pb grade of 79.31%. However, after adding Na_2SO_3, the Pb grade increased to 81.50%, but the yield in concentrate decreased to 46.50%. This result indicated that sulfite ions promoted the separation of galena from sphalerite. Fig. 6(b) illustrated the impact of sodium sulfite concentration on the separation of Pb–Zn mixed minerals with the addition of

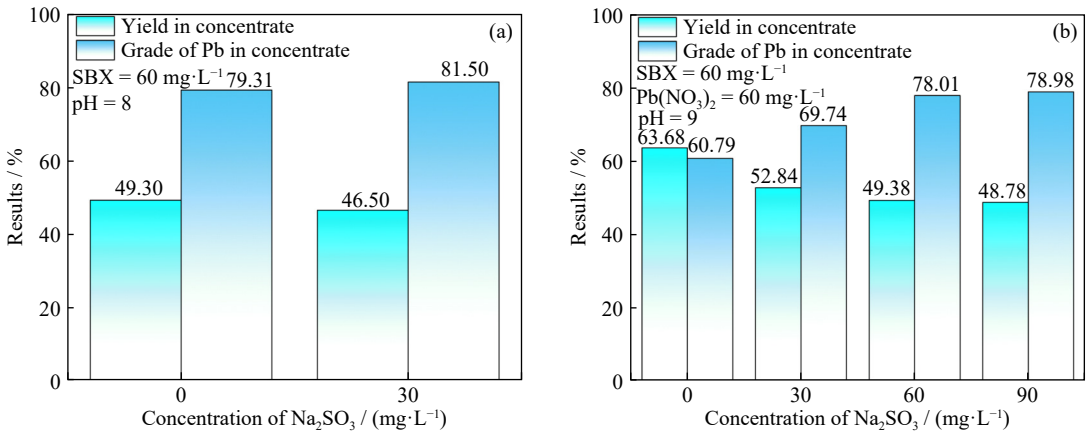

Fig. 6. Results of galena–sphalerite artificially mixed minerals: (a) without Pb^{2+}; (b) with Pb^{2+}.

60 mg/L $Pb(NO_3)_2$. As sodium sulfite concentration rose, the Pb grade in concentrate increased from 60.79% to 78.98%. However, the yield in concentrate gradually declined from 63.68% to 48.78%. Overall, these findings suggested that sulfite ions could counteract the influence of Pb^{2+} on sphalerite activation, benefiting the flotation separation of galena from sphalerite.

3.2. Contact angle measurement

The hydrophobicity of minerals could be determined by measuring the contact angle on their surfaces. Fig. 7 illustrated the contact angles of galena and sphalerite before and after treatment with sulfite ions and xanthate ions. Initially, the contact angles were 75.4° for galena and 41.3° for sphalerite, respectively [34–35]. After adding sodium sulfite, the contact angles decreased to 37.6° for sphalerite and 51.1° for galena, indicating that sulfite increased the hydrophobicity of both minerals, with galena remaining more hydrophobic than sphalerite. However, in the presence of xanthate, sulfite had a greater impact on the contact angle reduction of sphalerite compared to galena. With xanthate and sulfite, the contact angle on sphalerite decreased from 71.9° to 39.2°, while on galena it reduced from 98.4° to 90.0°. Thus, sulfite led to a significant decrease in hydrophobicity of sphalerite when both xanthate and sulfite were present, resulting in a greater difference in hydrophobicity between galena and sphalerite surfaces. Consequently, sulfite had a more significant effect on the difference of surface hydrophobicity between galena and sphalerite.

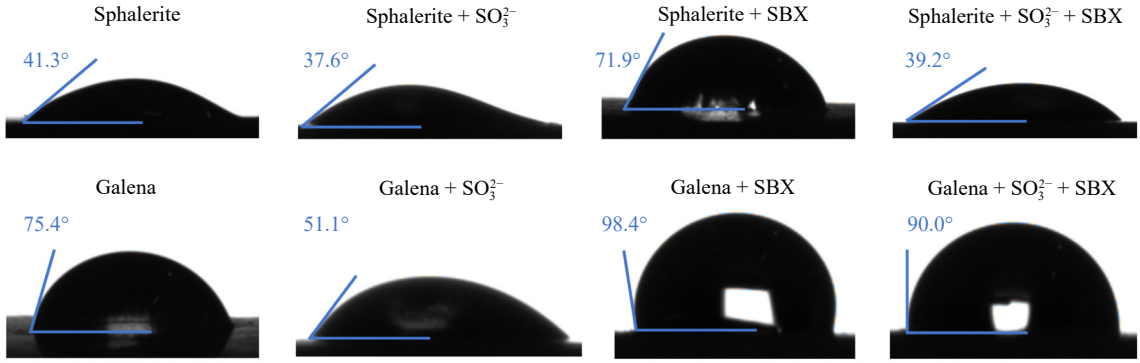

Fig. 7. Contact angles of galena and sphalerite before and after treatment with sulfite ions and xanthate ions.

3.3. Precipitation of Pb^{2+} and Zn^{2+} by sulfite

Fig. 8 showed the relationship between the precipitation amounts of Pb^{2+} and Zn^{2+} by sulfite ions and pH. Because Pb^{2+} began to precipitate at pH = 6, the amount of metal precipitated by sulfite could not be accurately determined. Therefore, the precipitation experiments only explored the precipitation of Pb^{2+} and Zn^{2+} within the pH range of 3–5. As shown in Fig. 8, it could be observed that sulfite ions had a strong precipitation ability towards Pb^{2+} within the entire pH range. Based on the concentration composition diagram, it could be inferred that this was caused by an increase in the concentration of SO_3^{2-} ions. However, sulfite ions did not precipitate zinc ions. At the pH range of 3–5, the precipitation amount of the entire Zn^{2+} was 0 mg, further indicating that sulfite could strongly precipitate Pb^{2+} in the solution, thereby eliminating the flotation of Pb^{2+} activated sphalerite.

3.4. UV–vis absorption spectra

Fig. 9(a) displayed the UV–vis absorption spectrum of SBX treated by different minerals with or without Na_2SO_3. The characteristic peak of xanthate in the UV–vis spectrum occurred at the wavelength of 301 nm [36–37]. In the untreated xanthate solution, this peak was the strongest. After treatment with sphalerite, the intensity of this peak slightly weakened, indicating that sphalerite had adsorption capacity

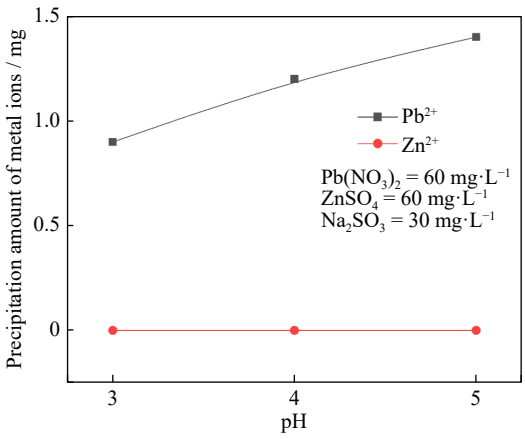

Fig. 8. Relationship between the precipitation amounts of Pb^{2+} and Zn^{2+} by sulfite ions and pH.

for xanthate. However, after treatment with galena, the intensity of the xanthate peak significantly decreased, indicating that galena had a strong adsorption capacity for xanthate. When sodium sulfite was added, new peak appeared in the solution. According to previous reports, sulfite and oxygen molecule jointly reacted with the xanthate ions in the solution, and a peak of perxanthate appeared (348 nm) [17,38–39]. After adding sodium sulfite, the peak of perxanthate in the xanthate solution treated with sphalerite was significantly stronger than that in the xanthate solution treated with galena, indicating xanthate in the sphalerite system was more easily decomposed by sulfite ions and oxygen molecule than in the galena system. However, after adding sulfite ions, the intensity of the xanthate peak in the treatment of galena slightly increased compared to the treatment of galena without sulfite ions. The sulfite ions had a certain desorption effect on the xanthate adsorbed on galena.

To further investigate the decomposition rate of xanthate in sphalerite and galena system by sulfite ions and oxygen, Fig. 9(b) showed the UV–vis absorption spectra of lead-xanthate and zinc-xanthate treated with sulfite. After mixing Pb^{2+} and xanthate, there was no peak of xanthate, indicating that xanthate ions and Pb^{2+} formed a stable complex, confirming the strong interaction between Pb^{2+} and xanthate ions. However, after mixing Zn^{2+} and xanthate, a strong peak of xanthate appeared, indicating that the interaction between xanthate ions and Zn^{2+} was weak. After adding sulfite to lead-xanthate, the characteristic peak of xanthate appeared, indicating that some of the xanthate bound to Pb^{2+} had been replaced by sulfite ions. In addition, a weak peak of perxanthate (348 nm) also appeared [17]. However, after adding sulfite to zinc-xanthate, the peak of xanthate treated by Zn^{2+} significantly weakened and the peak of perxanthate appeared significantly [17]. This result further confirmed that xanthate interacts more readily with sulfite ions and oxygen molecules within the sphalerite system than in the galena system, leading to the formation of perxanthate.

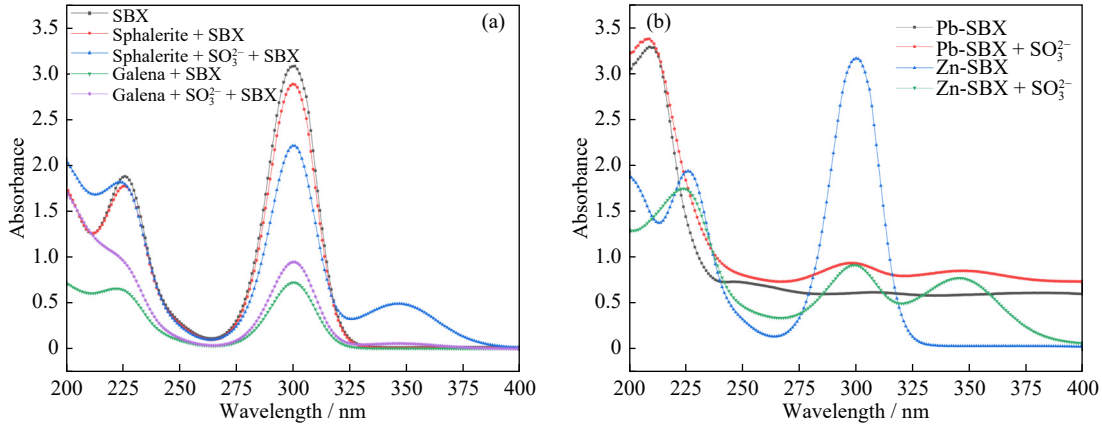

Fig. 9. UV–vis absorption spectrum of (a) SBX treated by different minerals with or without Na_2SO_3 and (b) lead-xanthate and zinc-xanthate treated with or without Na_2SO_3.

3.5. FTIR spectra

To further understanding the variations in flotation surface mechanisms of galena and sphalerite pre- and post-treatment with SBX and Na_2SO_3, FTIR spectra was depicted in Fig. 10. The FTIR spectra analysis provided valuable insights into the structural changes and surface interactions involved in the flotation process of galena and sphalerite upon treatment with SBX and Na_2SO_3. When the galena and sphalerite were treated by SBX, the peaks at 1029.4 and 1055.1 cm^{-1} corresponded to the C=S stretching vibration peak [40–41]. Furthermore, the symmetric and asymmetric C–O–C stretching vibrations were observed at the position of 1128.6 and 1170.7 cm^{-1} [37]. Meanwhile, the peak intensity on the surface of galena was substantially higher compared to sphalerite. Notably, upon the addition of sodium sulfite, the xanthate peak intensity on the surface of galena increased, indicating more xanthate was adsorbed on galena treated with sulfite ions. This phenomenon indicated that the addition of sodium sulfite was beneficial to the improvement of galena flotation recovery. Moreover, the peak observed at 1631.3 cm^{-1} could be attributed to moisture content [42–43]. After treatment with sulfite, the intensity of the moisture peak on the sphalerite surface was significantly enhanced. However, the intensity of the moisture peak on the galena's surface was significantly weakened. These findings demonstrated that

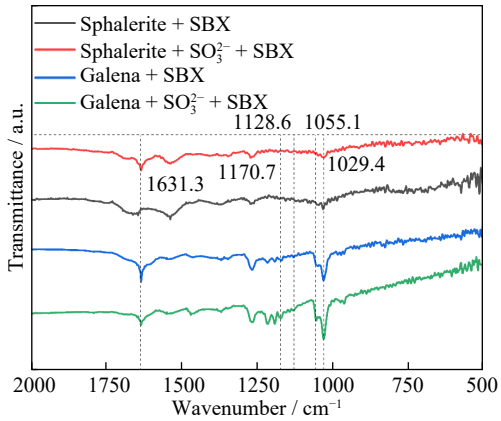

Fig. 10. FTIR spectra of galena and sphalerite before and after treatment with SBX and Na_2SO_3.

sulfite rendered the sphalerite surface more hydrophilic while making the galena surface more receptive to xanthate adsorption.

3.6. XPS analysis

Elemental compositions and chemical states could be obtained using XPS examination. The surface atomic concentrations of Pb, Zn, O, and S were summarized in Table 1. Fig. 11(a) showed that Pb, O, and S were detected in the surface of galena with or without Na_2SO_3. After treating with Na_2SO_3, the signals of Pb and S detected on the galena surface were strengthened, while the O signal was weakened. More specifically, the concentrations of Pb in the surface of galena increased from 14.0% to 21.4%. The concentrations of S increased from 42.8% to 52.6%, and the concentration of O decreased from 43.2% to 26.0%. After the surface of galena was treated with sodium sulfite, the lead content in the surface of galena significantly increased, meaning that more lead sites could be adsorbed by xanthate [15]. Therefore, in sulfite dosage flotation test, the recovery of galena increased with the increase of the amount of sulfite. Fig. 11(b) showed that Zn, O, and S were detected in the surface of sphalerite with or without Na_2SO_3. After treatment with Na_2SO_3, the signals of Zn and S detected in the sphalerite surface were obviously unchanged, while the O signal was strengthened. The concentrations of Zn in the surface of sphalerite increased from 32.4% to 32.5%. The concentrations of S decreased from 44.9% to 43.5%, and the concentration of O intensely increased from 22.7% to 24.0%. The increase in oxygen content in the surface of sphalerite meant that the surface of sphalerite treated with sulfite became more hydrophilic than without sodium sulfite. The XPS results indicated that sulfite ions increased the surface oxygen content of sphalerite, the hydrophilicity of sphalerite surface, and the difference in hydrophilicity between sphalerite and galena.

Table 1. Relative content of atoms in the surfaces of galena

at%

Minerals	Pb	Zn	O	S
PbS	14.0	—	43.2	42.8
PbS + SO_3^{2-}	21.4	—	26.0	52.6
ZnS	—	32.4	22.7	44.9
ZnS + SO_3^{2-}	—	32.5	24.0	43.5

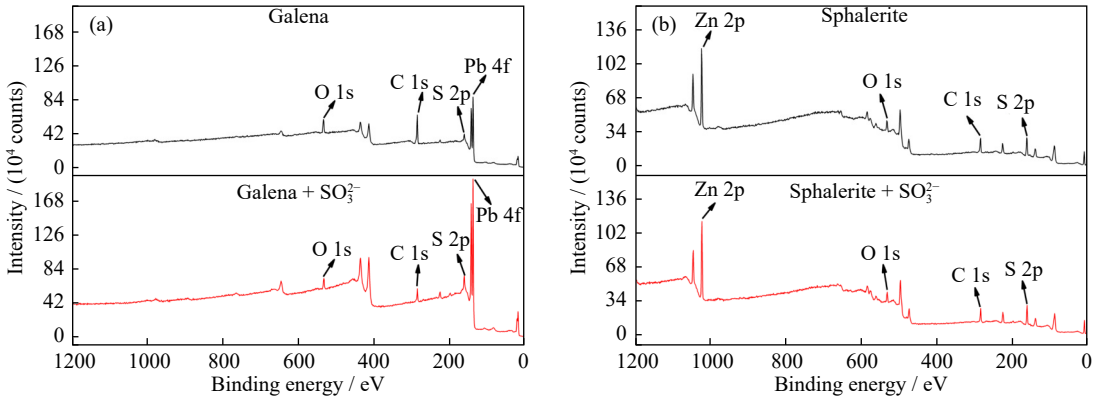

Fig. 11. XPS survey spectra of (a) galena and (b) sphalerite treated with 960 mg/L Na_2SO_3.

Fig. 12 showed the S 2p high-resolution XPS spectra of sphalerite before and after treatment with Na_2SO_3. As shown in Fig. 12, the peaks positioned at 161.80 and 162.95 eV were attributed to species S^{2-} [44–45]. After sodium sulfite treatment, no peaks of species SO_3^{2-} (166.00 eV) [46] were found, which indicated that SO_3^{2-} was was difficult to be adsorbed onto the surface of sphalerite.

3.7. Frontier molecular orbital analysis

Fig. 13 showed the frontier orbital shapes of sulfite ions, galena, and sphalerite. From Fig. 13(a), it could be seen that the lowest unoccupied molecular orbital (LUMO) of sulfite ion was σ orbit, therefore, sulfite ion was difficult to form feedback π bond with the π electron pairs of metal ions in mineral surface, but could form σ bond. However, it could be seen that the highest occupied molecular orbital (HOMO) of sulfite ion was mainly composed of three O 2p orbitals and S 3p orbitals, providing electrons (Fig. 13(d)).

The valence electron structure of Zn^{2+} is $3d^{10}4s^0$. From Fig. 13(b), it could be seen that the LUMO orbitals on the surface of sphalerite were mainly the 4s orbitals of zinc atoms. This was because the 4s orbitals in the valence electron layer of Zn^{2+} were empty orbitals. The 4s orbitals of Zn atoms on the surface of sphalerite could obtain lone pair elec-

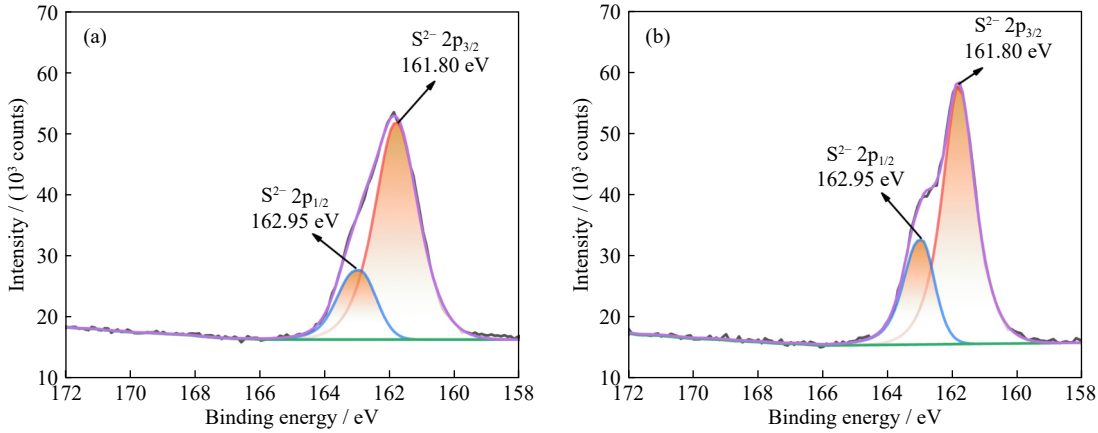

Fig. 12. S 2p high-resolution XPS spectra of (a) sphalerite and (b) sphalerite treated with Na_2SO_3.

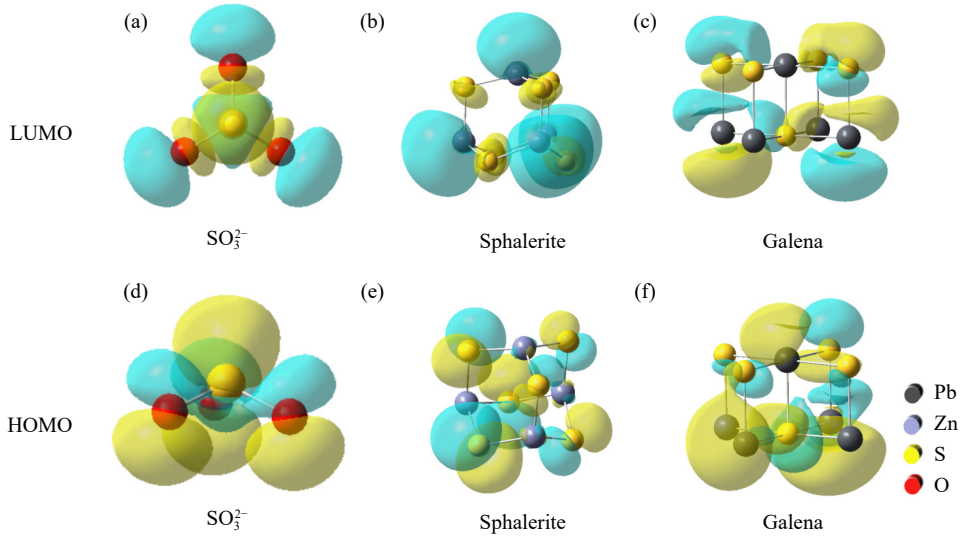

Fig. 13. Frontier orbital shapes of sulfite ion, galena, and sphalerite.

trons to form forward coordination. However, the LUMO orbital of Zn atom on the surface of sphalerite did not match the symmetry of the HOMO orbital of sulfite ion, resulting in only a weak positive coordination interaction between sulfite ion and the surface of sphalerite. From Fig. 13(e), it could be seen that the HOMO orbitals on the surface of sphalerite were mainly the 3p orbitals of sulfur atoms, with only a very small number of d orbitals on zinc atoms participating in the HOMO orbitals. $3d^{10}$ was the electron occupied state of zinc atoms, while $3d^{10}$ was a fully filled state with strong inertness. From the perspective of feedback π bonding, it was difficult for zinc atom on the surface of sphalerite to form feedback π bond with the LUMO orbital of sulfite ion.

The valence electron layer structure of Pb^{2+} in galena was $6s^26p^0$. From Fig. 13(c), it could be seen that the LUMO orbitals on the surface of galena were mainly composed of sulfur 3p orbitals, and the contribution of lead atoms was weak. The HOMO orbital of sulfite ion was difficult to effectively bond with the LUMO orbital of Pb atom on the surface of galena. As shown in Fig. 13(f), the HOMO orbitals on the surface of galena were mainly composed of the 6s orbital of lead and the 3p orbital of sulfur. These two types of orbits belong to the octahedral field σ orbit. The HOMO orbital of lead on the surface of galena and the LUMO orbital of sulfite ion could effectively form σ (s–p) bond. Based on the above analysis, it further indicated that sulfite ion was difficult to adsorb on sphalerite, while it was more strongly adsorbed on galena.

3.8. DFT calculations

Table 2 showed the adsorption energies of various adsorbates on sphalerite and galena. Table 3 showed the average bond lengths of adsorbates on the surfaces of sphalerite and galena. As illustrated in Fig. 14(a) and (b), the adsorption of SO_3^{2-} on the surfaces of sphalerite and galena resulted in the Zn–S bond distance was 3.661 Å and the Pb–S bond distance was 3.001 Å. The corresponding adsorption energies of SO_3^{2-} were −16.7 and −32.3 kJ/mol, respectively. As shown in Fig. 14(c) and (d), the adsorption energy of H_2O on the surface Zn site was −60.6 kJ/mol, with Zn–O bond length of 2.138 Å. While the adsorption energy on the Pb site was −19.7 kJ/mol, with Pb–O bond length of 2.864 Å [46]. The adsorption energy of H_2O on the Zn sites was lower than that on the Pb sites, which clarified that the adsorption of H_2O on the surface Zn sites was more spontaneous than that on the surface Pb sites. In addition, sulfite ions and lead ions generated hydrophilic $PbSO_3$. The adsorption energy of $PbSO_3$ on sphalerite was −235.5 kJ/mol, and the average length of S–Pb and O–Zn bond on the surface sphalerite was 2.294 Å. While

Table 2. Adsorption energies of adsorbates on the surfaces of sphalerite (110) and galena (100) (kJ·mol^{-1})

Adsorbates	Sphalerite	Galena
SO_3^{2-}	−16.7	−32.3
H_2O	−60.6	−19.7
$PbSO_3$	−235.5	−175.6

Table 3. Average bond lengths of adsorbates on the surfaces of sphalerite (110) and galena (100) Å

Adsorbates	Sphalerite	Galena
SO_3^{2-}	3.661	3.001
H_2O	2.138	2.864
$PbSO_3$	2.294	2.540

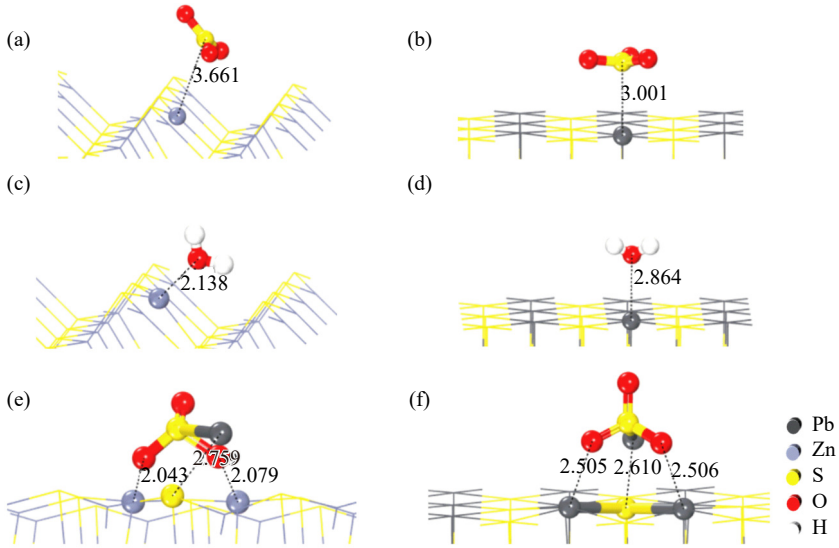

Fig. 14. Adsorption configurations of adsorbates on the surface of sphalerite (110) and galena (100): (a) SO_3^{2-} on sphalerite; (b) SO_3^{2-} on galena; (c) OH^- on sphalerite; (d) OH^- on galena; (e) $PbSO_3$ on sphalerite; (f) $PbSO_3$ on galena.

the adsorption energy of $PbSO_3$ on galena was −175.6 kJ/mol and the average length of the S–Pb and O–Pb bond on the surface of galena was 2.540 Å. This result indicated that $PbSO_3$ was more easily be adsorbed on the surface of sphalerite, further reducing its floatability. Hence, in the flotation separation of galena from sphalerite, sulfite could effectively depress lead ions activated sphalerite.

3.9. Mechanism diagram of sulfite depressing sphalerite and Pb^{2+} activated sphalerite

According to the previous analysis results, schematic of the mechanism by which sulfite ions depressed sphalerite and Pb^{2+} activated sphalerite was shown in Fig. 15. As shown in Fig. 15(a), the adsorption of sulfite ions on the surface of sphalerite was weak, making it difficult to depress sphalerite. However, sulfite ions could increase the oxygen content on the surface of sphalerite, enhanced its hydrophilicity, and further increased the difference in hydrophilicity between sphalerite and galena. In addition, in the presence of sulfite ions, the xanthate in the sphalerite system was more easily decomposed into perxanthate than the xanthate in the galena system. As shown in Fig. 15(b), sulfite ions could chelate Pb^{2+} in the solution, and the generated $PbSO_3$ was more easily be adsorbed on the surface of sphalerite, further depressing Pb^{2+} activated sphalerite. This diagram provided clearer understanding of the depression mechanism of sulfite ions on sphalerite and Pb^{2+} activated sphalerite in the flotation separation of galena from sphalerite.

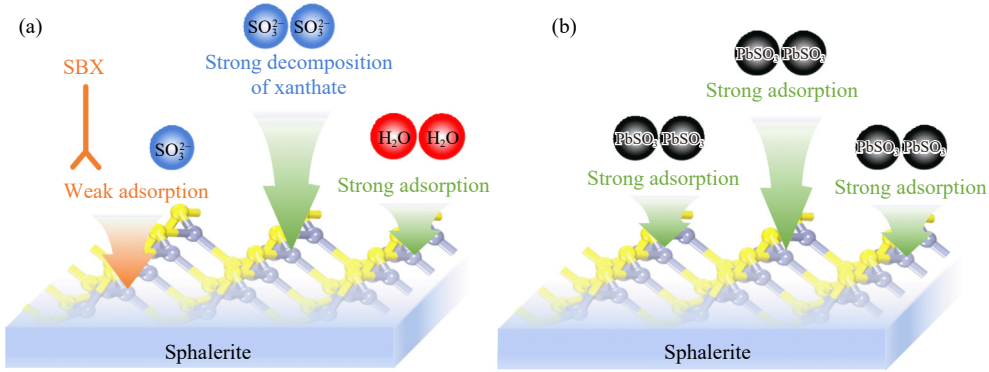

Fig. 15. Diagram of sulfite depression mechanism: (a) sphalerite; (b) Pb^{2+} activated sphalerite.

4. Conclusions

Sulfite ions acted as depressants of sphalerite in the flotation separation of galena from sphalerite. The single and mixed mineral experimental results indicated that sulfite ions could depress sphalerite and Pb^{2+} activated sphalerite. The

contact angle, UV–vis spectrum, ICP-OES, FTIR spectroscopy, XPS, Frontier molecular orbital analysis, and DFT calculations further revealed the sophisticated depression mechanism of sulfite ions on sphalerite and Pb^{2+} activated sphalerite in the flotation separation of galena from sphalerite. The main conclusions are as follows:

(1) The high-resolution XPS spectra of sphalerite S 2p after SO_3^{2-} treatment showed no SO_3^{2-} peaks was detected. The DFT calculation results also indicated that the adsorption of SO_3^{2-} on sphalerite was weak, with an adsorption energy of only −16.7 kJ/mol. Frontier molecular orbital analysis further indicated that sulfite ions were difficult to be adsorb on sphalerite surface.

(2) The oxygen content in the surface of sphalerite treated with sulfite ions increased, which enhanced the hydrophilicity of the sphalerite surface and further increased the difference in hydrophilicity between sphalerite and galena. DFT calculations further indicated that H_2O was more easily be adsorbed on the surface of sphalerite. The adsorption energy of H_2O on the surface of sphalerite was −60.6 kJ/mol, which was much lower than that on the surface of galena.

(3) Sulfite ions could precipitate lead ions, reducing the influence of lead ions on the activation of sphalerite. DFT calculations further indicated that $PbSO_3$ was more easily be adsorbed on the surface of sphalerite. The adsorption energy of $PbSO_3$ on the surface of sphalerite was −235.5 kJ/mol, which was 59.9 kJ/mol lower than that on the surface of galena.

(4) The UV–vis spectrum showed that after adding sulfite ions, the peak of perxanthate in the sphalerite treated with xanthate solution was significantly stronger than that in the galena treated with xanthate solution. The results indicated that xanthate interacted more readily with sulfite ions and oxygen molecules within the sphalerite system, leading to the formation of perxanthate.

In summary, based on the results of experiments and DFT calculations, the depression mechanism of sulfite ions on sphalerite and Pb^{2+} activated sphalerite in the flotation separation of galena from sphalerite was elucidated, facilitating a deeper understanding of the action principles of the flotation reagents at the mineral interface and advancing the development of fundamental theories in mineral flotation.

Acknowledgements

This work was financially supported by the National Natural Science Foundation of China (No. 52074356), Open Foundation of State Key Laboratory of Mineral Processing (No. BGRIMM-KJSKL-2023-06), the National Key R&D Program of China (No. 2022YFC2904500), the Science and Technology Innovation Program of Hunan Province, China (No. 2022RC1183), Changsha Science and Technology Project, China (Outstanding Innovative Youth Training Program), Innovation driven program of Central South University (No. 2023CXQD002), National 111 Project (No. B14034), and the Fundamental Research Funds for the Central Universities of Central South University Project (No. 50621747). This work was carried out in part using hardware and/or software provided by the Computing Platform of Mineral Processing Computational Chemistry at School of Mineral Processing and Bioengineering of Central South University, the High-Performance Computing Centers of Central South University, and Tianhe II supercomputer at the National Supercomputing Center in Guangzhou, China.

Conflict of Interest

The authors declare that they have no financial or proprietary interests that influence the reporting of this article.

References

[1] C. Xue and Z.C. Wei, Reaction mechanism and research progress of depressants in sphalerite flotation, *Multipurp. Util. Miner. Resour.*, (2017), No. 3, p. 38.

[2] T.S. Qiu, Q.M. Nie, Y.Q. He, and Q.Z. Yuan, Density functional theory study of cyanide adsorption on the sphalerite (1 1 0) surface, *Appl. Surf. Sci.*, 465(2019), p. 678.

[3] B. Guo, Y.J. Peng, and R. Espinosa-Gomez, Cyanide chemistry and its effect on mineral flotation, *Miner. Eng.*, 66-68(2014), p. 25.

[4] Y.F. Mu, Y.J. Peng, and R.A. Lauten, The depression of pyrite in selective flotation by different reagent systems–A Literature review, *Miner. Eng.*, 96-97(2016), p. 143.

[5] T.H. Pak, T.C. Sun, C.Y. Xu, and Y.H. Jo, Flotation and surface modification characteristics of galena, sphalerite and pyrite in collecting-depressing-reactivating system, *J. Cent. South Univ.*, 19(2012), No. 6, p. 1702.

[6] P. Clarke, P. Arora, D. Fornasiero, J. Ralston, and R.S.C. Smart, Separation of chalcopyrite or galena from sphalerite: A flotation and X-ray photoelectron spectroscopic study, [in] S.P. Mehrotra, ed., *Mineral Processing*: *Recent Advances and Future Trends*, Allied Publishers Limited New Delhi, New Delhi, 1995, p. 369.

[7] S.G. Malghan, Role of sodium sulfide in the flotation of oxidized copper, lead, and zinc ores, *Min. Metall. Explor.*, 3(1986), No. 3, p. 158.

[8] V.A. Bocharov, V.A. Ignatkina, and A.A. Kayumov, Rational separation of complex copper–zinc concentrates of sulfide ore, *J. Min. Sci.*, 52(2016), No. 4, p. 793.

[9] E. E. Öz, *Evaluation of Kosovo-Artana Concentrator Tailings* [Dissertation], Middle East Technical University, Ankara, 2011.

[10] L.M. Zhang, J.D. Gao, S.A. Khoso, *et al*., A reagent scheme for galena/sphalerite flotation separation: Insights from first-principles calculations, *Miner. Eng.*, 167(2021), art. No. 106885.

[11] T.N. Khmeleva, J.K. Chapelet, W.M. Skinner, and D.A. Beattie, Depression mechanisms of sodium bisulphite in the xanthate-induced flotation of copper activated sphalerite, *Int. J. Miner. Process.*, 79(2006), No. 1, p. 61.

[12] T.N. Khmeleva, W. Skinner, and D.A. Beattie, Depressing mechanisms of sodium bisulphite in the collectorless flotation of copper-activated sphalerite, *Int. J. Miner. Process.*, 76(2005), No. 1, p. 43.

[13] W.Z. Shen, D. Fornasiero, and J. Ralston, Flotation of sphalerite and pyrite in the presence of sodium sulfite, *Int. J. Miner. Process.*, 63(2001), No. 1, p. 17.

[14] T.N. Khmeleva, W. Skinner, D.A. Beattie, and T.V. Georgiev, The effect of sulphite on the xanthate-induced flotation of copper-activated pyrite, *Physicochem. Probl. Miner. Process.*, 36(2002), p. 185.

[15] S.R. Grano, C.A. Prestidge, and J. Ralston, Sulphite modifica-

tion of galena surfaces and its effect on flotation and xanthate adsorption, *Int. J. Miner. Process.*, 52(1997), No. 1, p. 1.
[16] J. Gustafsson, Visual MINTEQ Rev. 3.1, 2007.
[17] Z.C. Pan, Z.C. Liu, J.J. Xiong, *et al*., Application and depression mechanism of sodium sulfite on galena–pyrite mixed concentrate flotation separation: Huize lead–zinc mine, China, as an example, *Miner. Eng.*, 185(2022), art. No. 107696.
[18] M.D. Segall, P.J.D. Lindan, M.J. Probert, *et al*., First-principles simulation: Ideas, illustrations and the CASTEP code, *J. Phys.: Condens. Matter*, 14(2002), No. 11, p. 2717.
[19] J.P. Perdew, K. Burke, and Y. Wang, Generalized gradient approximation for the exchange-correlation hole of a many-electron system, *Phys. Rev. B: Condens. Matter*, 54(1996), No. 23, p. 16533.
[20] Y.J. Luo, L.M. Ou, J.H. Chen, *et al*., Hydration mechanisms of smithsonite from DFT-D calculations and MD simulations, *Int. J. Min. Sci. Technol.*, 32(2022), No. 3, p. 605.
[21] T. Bučko, S. Lebègue, J. Hafner, and J.G. Ángyán, Tkatchenko-Scheffler van der Waals correction method with and without self-consistent screening applied to solids, *Phys. Rev. B*, 87(2013), No. 6, art. No. 064110.
[22] K. Wright, G.W. Watson, S.C. Parker, and D.J. Vaughan, Simulation of the structure and stability of sphalerite (ZnS) surfaces, *Am. Mineral.*, 83(1998), No. 1-2, p. 141.
[23] J.H. Chen, Y. Chen, and Y.Q. Li, Effect of vacancy defects on electronic properties and activation of sphalerite (110) surface by first-principles, *Trans. Nonferrous Met. Soc. China*, 20(2010), No. 3, p. 502.
[24] H.M. Steele, K. Wright, and I.H. Hillier, A quantum-mechanical study of the (110) surface of sphalerite (ZnS) and its interaction with Pb^{2+} species, *Phys. Chem. Miner.*, 30(2003), No. 2, p. 69.
[25] J.H. Chen, X.H. Long, and Y. Chen, Comparison of multilayer water adsorption on the hydrophobic galena (PbS) and hydrophilic pyrite (FeS_2) surfaces: A DFT study, *J. Phys. Chem. C*, 118(2014), No. 22, p. 11657.
[26] J.A. Tossell and D.J. Vaughan, Electronic structure and the chemical reactivity of the surface of galena, *Can. Mineral.*, 25(1987), No. 3, p. 381.
[27] H.L. Zhang, W. Sun, C.Y. Zhang, J.Y. He, D.X. Chen, and Y.G. Zhu, Adsorption performance and mechanism of the commonly used collectors with oxygen-containing functional group on the ilmenite surface: A DFT study, *J. Mol. Liq.*, 346(2022), art. No. 117829.
[28] H.L. Zhang, W. Sun, Y.G. Zhu, J.Y. He, D.X. Chen, and C.Y. Zhang, Effects of the goethite surface hydration microstructure on the adsorption of the collectors dodecylamine and sodium oleate, *Langmuir*, 37(2021), No. 33, p. 10052.
[29] C.C. Sui, D. Lee, A. Casuge, and J.A. Finch, Comparison of the activation of sphalerite by copper and lead, *Min. Metall. Explor.*, 16(1999), No. 3, p. 53.
[30] A.R. Gerson, A.G. Lange, K.E. Prince, and R.S.C. Smart, The mechanism of copper activation of sphalerite, *Appl. Surf. Sci.*, 137(1999), No. 1-4, p. 207.
[31] G.S. Reddy and C.K. Reddy, The chemistry of activation of sphalerite–A review, *Miner. Process. Extr. Metall. Rev.*, 4(1988), No. 1-2, p. 1.
[32] J. Liu, M. Ejtemaei, A.V. Nguyen, S.M. Wen, and Y. Zeng, Surface chemistry of Pb-activated sphalerite, *Miner. Eng.*, 145(2020), art. No. 106058.
[33] Z.Y. Zhang, S. Liu, F.Y. Liu, M. Mohamed Mohamed Ahmed, X.Y. Qu, and G.Y. Liu, The flotation separation of sphalerite from pyrite through a novel flotation reagent system of $FeCl_3$–$CuSO_4$-aminotriazolethione, *J. Mol. Liq.*, 345(2022), art. No. 116997.
[34] B. Jańczuk, W. Wójcik, A. Zdziennicka, and F. González-Caballero, Components of surface free energy of galena, *J. Mater. Sci.*, 27(1992), No. 23, p. 6447.
[35] R. Woods, C.I. Basilio, D.S. Kim, and R.H. Yoon, Chemisorption of ethyl xanthate on copper electrodes, *Int. J. Miner. Process.*, 42(1994), No. 3-4, p. 215.
[36] Z. Wang, Y.L. Qian, L.H. Xu, B. Dai, J.H. Xiao, and K.B. Fu, Selective chalcopyrite flotation from pyrite with glycerine–xanthate as depressant, *Miner. Eng.*, 74(2015), p. 86.
[37] T. Yamamoto, Mechanism of pyrite depression by sulfite in the presence of sphalerite, *Complex Sulphide Ores*, 1980.
[38] S.R. Grano, C.A. Prestidge, and J. Ralston, Solution interaction of ethyl xanthate and sulphite and its effect on galena flotation and xanthate adsorption, *Int. J. Miner. Process.*, 52(1997), No. 2-3, p. 161.
[39] Y.H. Zhang, Z. Cao, Y.D. Cao, and C.Y. Sun, FTIR studies of xanthate adsorption on chalcopyrite, pentlandite and pyrite surfaces, *J. Mol. Struct.*, 1048(2013), p. 434.
[40] W.X. Huang, R.H. Liu, F. Jiang, H.H. Tang, L. Wang, and W. Sun, Adsorption mechanism of 3-mercaptopropionic acid as a chalcopyrite depressant in chalcopyrite and galena separation flotation, *Colloids Surf. A*, 641(2022), art. No. 128063.
[41] Z.B. Deng, W.L. Cheng, Y. Tang, X. Tong, and Z.H. Liu, Adsorption mechanism of copper xanthate on pyrite surfaces, *Physicochem. Probl. Miner. Process.*, 57(2021), No. 3, p. 46.
[42] K.L. Zhao, W. Yan, X.H. Wang, B. Hui, G.H. Gu, and H. Wang, The flotation separation of pyrite from pyrophyllite using oxidized guar gum as depressant, *Int. J. Miner. Process.*, 161(2017), p. 78.
[43] U. Becker and M.F. Hochella, The calculation of STM images, STS spectra, and XPS peak shifts for galena: New tools for understanding mineral surface chemistry, *Geochim. Cosmochim. Acta*, 60(1996), No. 13, p. 2413.
[44] H.Y. Xie, Y.H. Liu, B. Rao, *et al*., Selective passivation behavior of galena surface by sulfuric acid and a novel flotation separation method for copper–lead sulfide ore without collector and inhibitor, *Sep. Purif. Technol.*, 267(2021), art. No. 118621.
[45] S. Yagi, M. Nambu, C. Tsukada, *et al*., Spectral studies on sulfur poisoning of Pd/Mg_6Ni by NEXAFS and XPS, *Appl. Surf. Sci.*, 267(2013), p. 45.
[46] F. Zhang, W. Sun, H.L. Zhang, *et al*., Selective adsorption mechanism of zinc ions on the surfaces of galena and sphalerite in the flotation separation of Pb–Zn, *JOM*, 75(2023), No. 11, p. 4808.